Cell Reports Medicine, Volume *4*

Supplemental information

Targeting the TCA cycle through cuproptosis confers synthetic lethality on ARID1A-deficient hepatocellular carcinoma

Tao Xing, Li Li, Yiran Chen, Gaoda Ju, Guilan Li, Xiaoyun Zhu, Yubo Ren, Jing Zhao, Zhilei Cheng, Yan Li, Da Xu, and Jun Liang

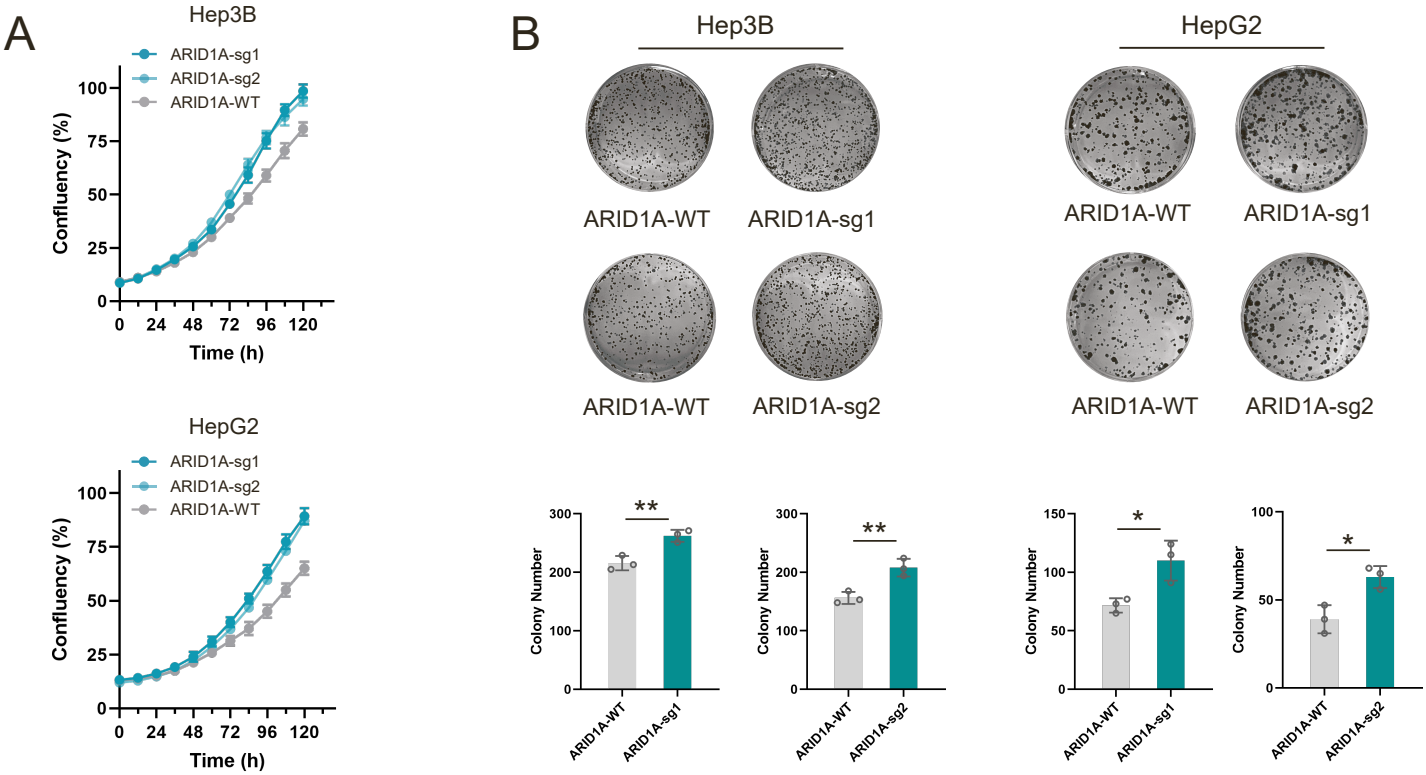

Supplementary Figure S1. ARID1A deficiency enhanced tumorigenicity in HCC, related to Figure 1

(A) Growth curves measured by IncuCyte® Live-Cell Analysis Imaging System in ARID1A knockout and control cells (mean ±SD; n=3 independent experiments).

(B) Colony formation and quantification in parental and ARID1A knockout cells cultivated for a duration of 10 to 15 days (mean ±SD; n=3 independent experiments).

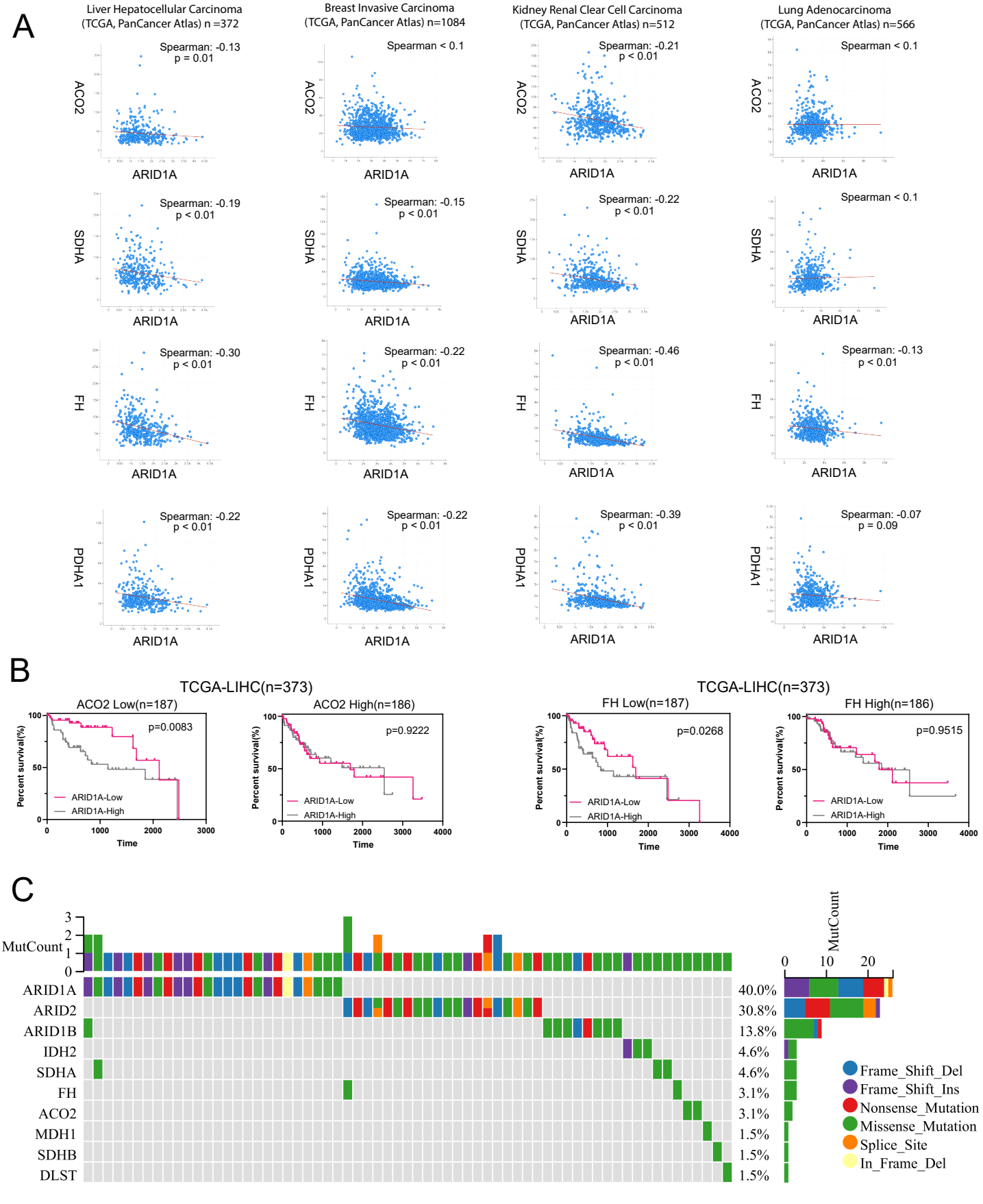

Supplementary Figure S2. ARID1A deficiency engendered a reliance on genes associated with the TCA cycle, related to Figure 2

(A) ARID1A expression was significantly correlated with an increase in the expression of TCA cycle genes across multiple cancer types.

(B) Kaplan–Meier curves demonstrating that low ARID1A and ACO2 or FH mRNA expression levels were correlated with better prognosis in HCC patients in the TCGA cohort.

(C) Alterations in SWI/SNF subunit and TCA-related genes in HCC within the TCGA dataset.

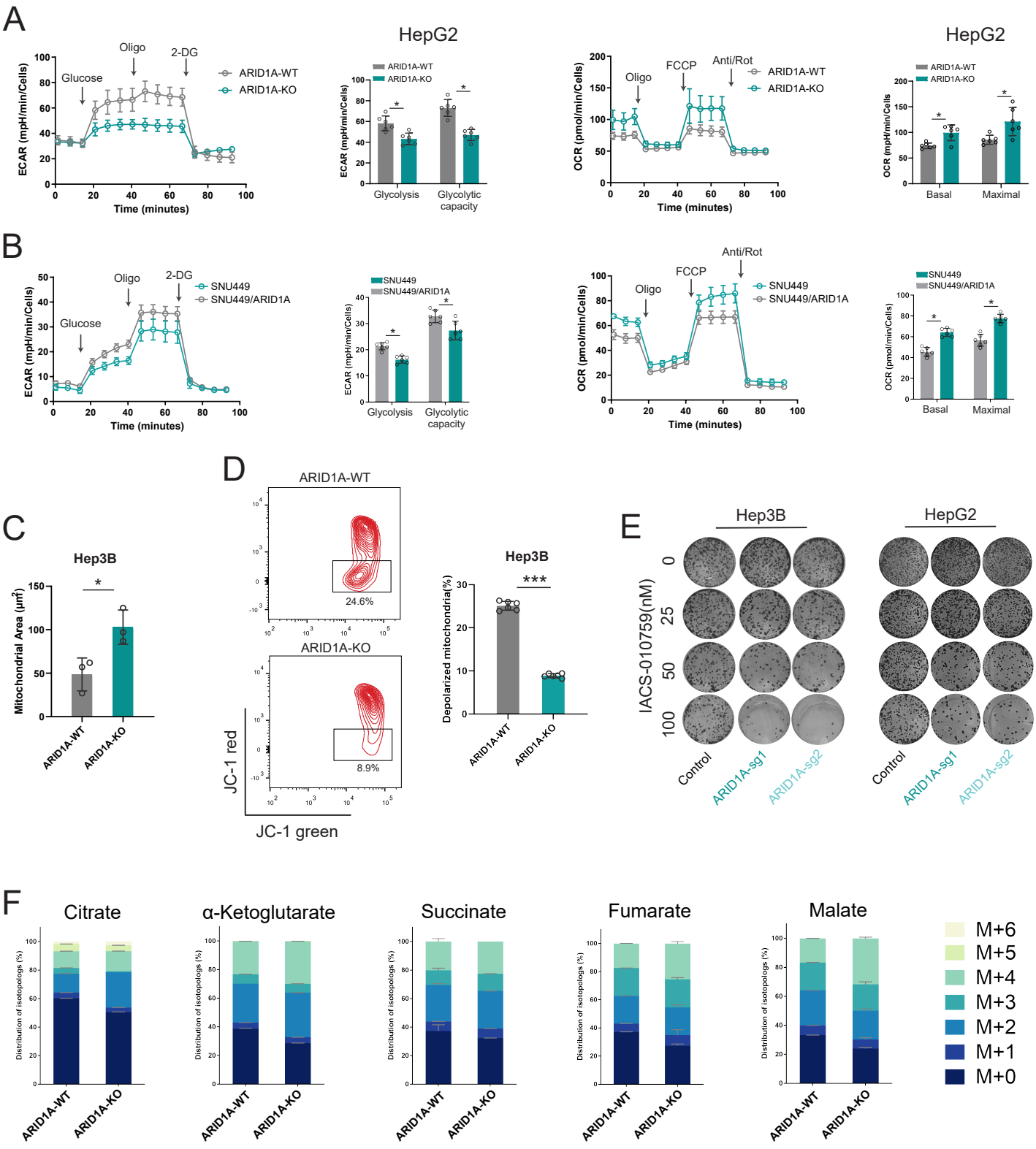

Supplementary Figure S3. ARID1A loss in HCC cells results in impaired glycolysis and increased dependence on mitochondrial respiration, related to Figure 3

(A-B) Seahorse glycolysis stress test and mito stress test in indicated cell lines (mean ±SD; n=6 independent experiments).

(C) Quantification of mitochondrial area in parental and ARID1A-KO (sg1) Hep3B cells (mean ±SD; n=3 independent experiments).

(D) JC-1 staining was conducted to evaluate the mitochondrial membrane potential in parental and ARID1A-KO (sg1) Hep3B cells (mean ±SD; n=6 independent experiments).

(E) Colony formation assay of parental and ARID1A knockout cells treated with IACS-010759 for 10–15 days (mean ±SD; n=3 independent experiments).

(F) Fractional labelling of TCA cycle intermediates (mean ±SD; n=3 independent experiments).

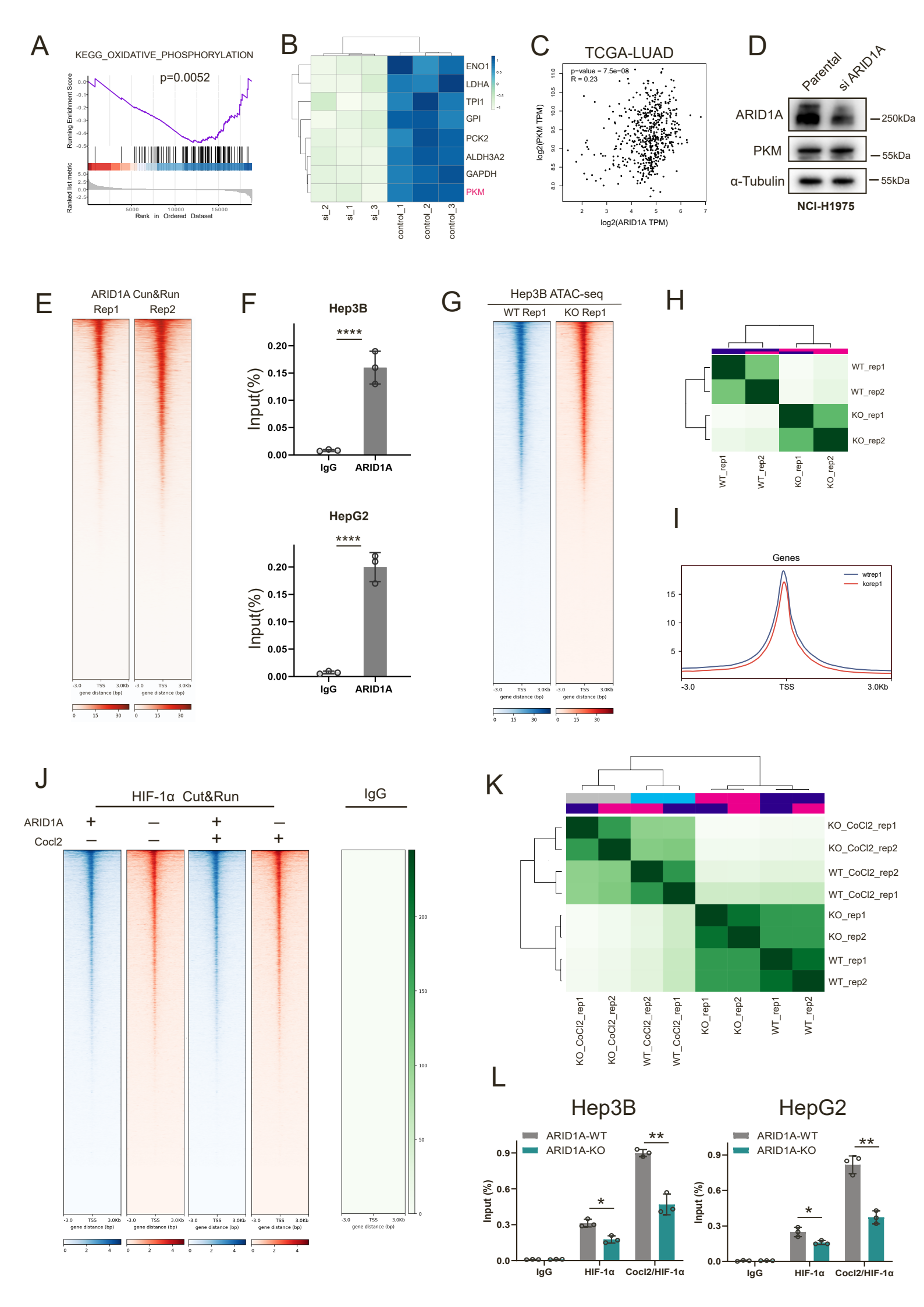
A
KEGG_OXIDATIVE_PHOSPHORYLATION
p=0.0052
Running Enrichment Score
Ranked list metric
Rank in Ordered Dataset
B
ENO1
LDHA
TPI1
GPI
PCK2
ALDH3A2
GAPDH
PKM
si_2
si_1
si_3
control_1
control_2
control_3
C
TCGA-LUAD
p−value = 7.5e−08
R = 0.23
log2(PKM TPM)
log2(ARID1A TPM)
D
Parental
si ARID1A
ARID1A
PKM
α-Tubulin
250kDa
55kDa
55kDa
NCI-H1975
E
ARID1A Cun&Run
Rep1
Rep2
gene distance (bp)
F
Hep3B
****
Input(%)
IgG
ARID1A
HepG2
****
Input(%)
IgG
ARID1A
G
Hep3B ATAC-seq
WT Rep1
KO Rep1
gene distance (bp)
H
WT_rep1
WT_rep2
KO_rep1
KO_rep2
I
Genes
wtrep1
korep1
-3.0
TSS
3.0Kb
J
HIF-1α Cut&Run
IgG
ARID1A
Cocl2
gene distance (bp)
K
KO_CoCl2_rep1
KO_CoCl2_rep2
WT_CoCl2_rep2
WT_CoCl2_rep1
KO_rep1
KO_rep2
WT_rep1
WT_rep2
L
Hep3B
HepG2
ARID1A-WT
ARID1A-KO
Input (%)
IgG
HIF-1α
Cocl2/HIF-1α

Supplementary Figure S4. ARID1A deficiency suppressed PKM transcription, related to Figure 4

(A) GSEA revealed that the oxidative phosphorylation pathway-associated genes were significantly upregulated in HepG2 ARID1A-knockdown cells.

(B) Expression of glycolysis-related genes in control and ARID1A knockdown HepG2 cells, as determined by RNA-seq analysis (n=3 independent experiments).

(C) The mRNA level of PKM exhibited a positive correlation with that of ARID1A in the TCGA lung adenocarcinoma dataset,

(D) Parental and ARID1A knockdown NCI-H1975 lung cancer cells were examined for the expression of PKM by immunoblotting

(E) Heatmap displaying the ARID1A Cut&Run reads distribution at the transcription start sites (TSS) in Hep3B cells.

(F) Cut&Run-qPCR analysis of recruitment of ARID1A at the promoters of PKM. (mean ±SD; n=3 independent experiments).

(G) Heatmap of ATAC-seq reads distribution.

(H) Heatmap presents the clustering of ATAC-seq.

(I) Signal intensity plot demonstrating genome-wide comparison of chromatin accessibility.

(J) Heatmap showing the Cut&Run reads distribution at the transcription start sites (TSS) of HIF-1α under varying growth conditions.

(K) Heatmap displaying clustering of Cut&Run binding peaks of HIF-1α under different growth conditions.

(L) Cut&Run-qPCR analysis of HIF-1α recruitment to the promoter of PKM under different growth conditions in parental and ARID1A-KO cells (mean ±SD; n=3 independent experiments).

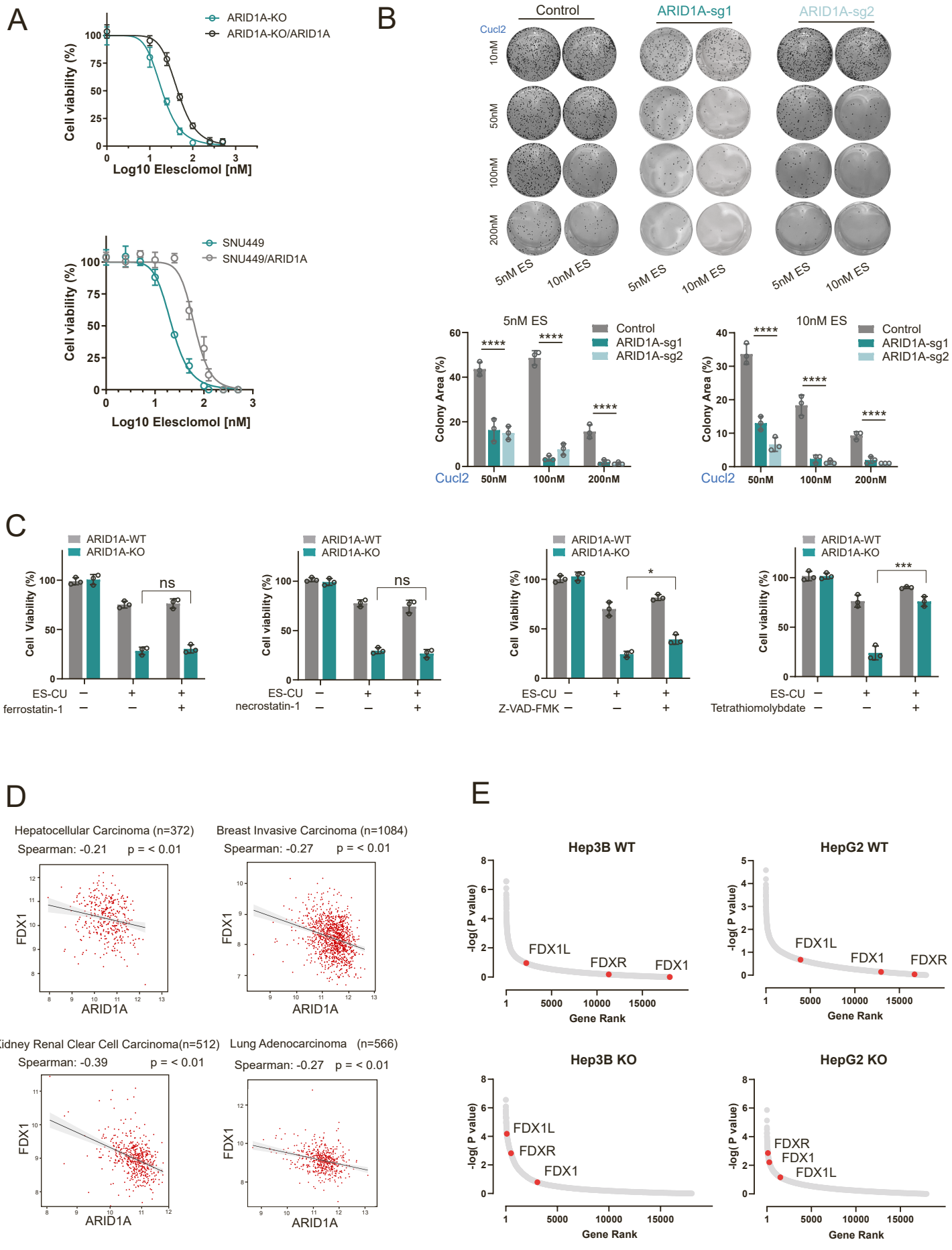
A
ARID1A-KO
ARID1A-KO/ARID1A
Cell viability (%)
Log10 Elesclomol [nM]
SNU449
SNU449/ARID1A
B
Control
ARID1A-sg1
ARID1A-sg2
Cucl2
10nM
50nM
100nM
200nM
5nM ES
10nM ES
Colony Area (%)
C
ARID1A-WT
ARID1A-KO
Cell Viability (%)
ns
ES-CU
ferrostatin-1
necrostatin-1
Z-VAD-FMK
Tetrathiomolybdate
D
Hepatocellular Carcinoma (n=372)
Spearman: -0.21 p = < 0.01
Breast Invasive Carcinoma (n=1084)
Spearman: -0.27 p = < 0.01
Kidney Renal Clear Cell Carcinoma(n=512)
Spearman: -0.39 p = < 0.01
Lung Adenocarcinoma (n=566)
Spearman: -0.27 p = < 0.01
FDX1
ARID1A
E
Hep3B WT
HepG2 WT
Hep3B KO
HepG2 KO
-log(P value)
FDX1L
FDXR
FDX1
Gene Rank

Supplementary Figure S5. ARID1A deficiency sensitized cells to cuproptosis in vitro, related to Figure 5

(A) The reduction in elesclomol (with 1 μM $CuCl_2$ in media) IC50 values could be mitigated through the restoration of ARID1A in ARID1A-KO (sg1) Hep3B or SNU449 cells (mean ±SD; n=6 independent experiments).

(B) Colony formation assay of Hep3B cells treated with different concentrations of elesclomol and $CuCl_2$ for 10–15 days (mean ±SD; n=3 independent experiments).

(C) Parental and ARID1A-KO (sg1) Hep3B cells were treated with 25 nM elesclomol (with 1 μM $CuCl_2$ in media) together with or without inhibitors (Z-VAD-FMK, 10 μM; Necrostatin-1, 10 μM; Ferrostatin-1, 10 μM; Tetrathiomolybdate, 10μM) for 48h, cell viability was subsequently evaluated (mean ±SD; n=3 independent experiments).

(D) Analysis of the TCGA database revealed the negative correlation between ARID1A and FDX1 mRNA expression across multiple cancer types.

(E) Dot plot showing noteworthy synthetic lethality observed between FDX1, FDXR, and FDX1L with ARID1A.

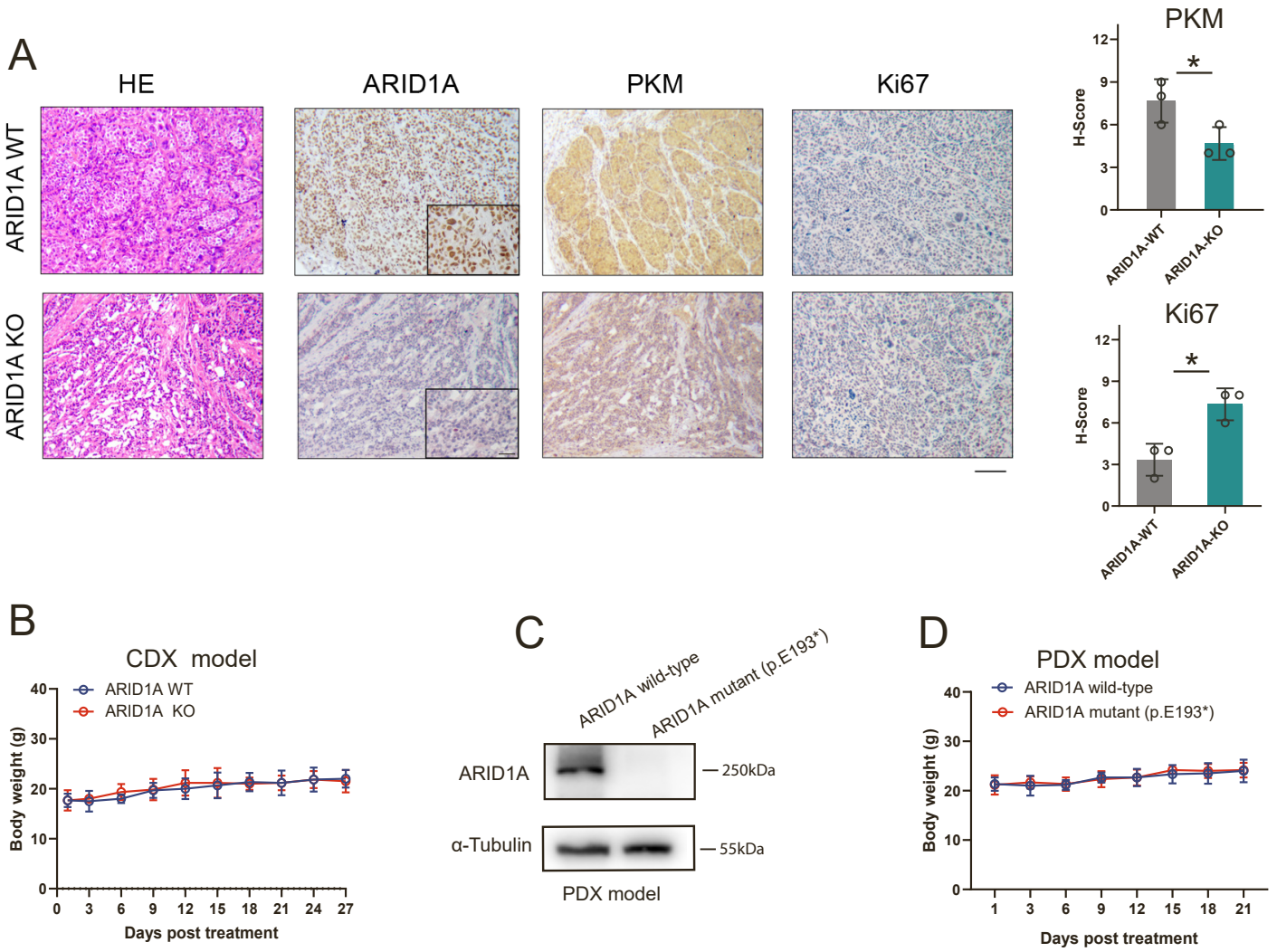

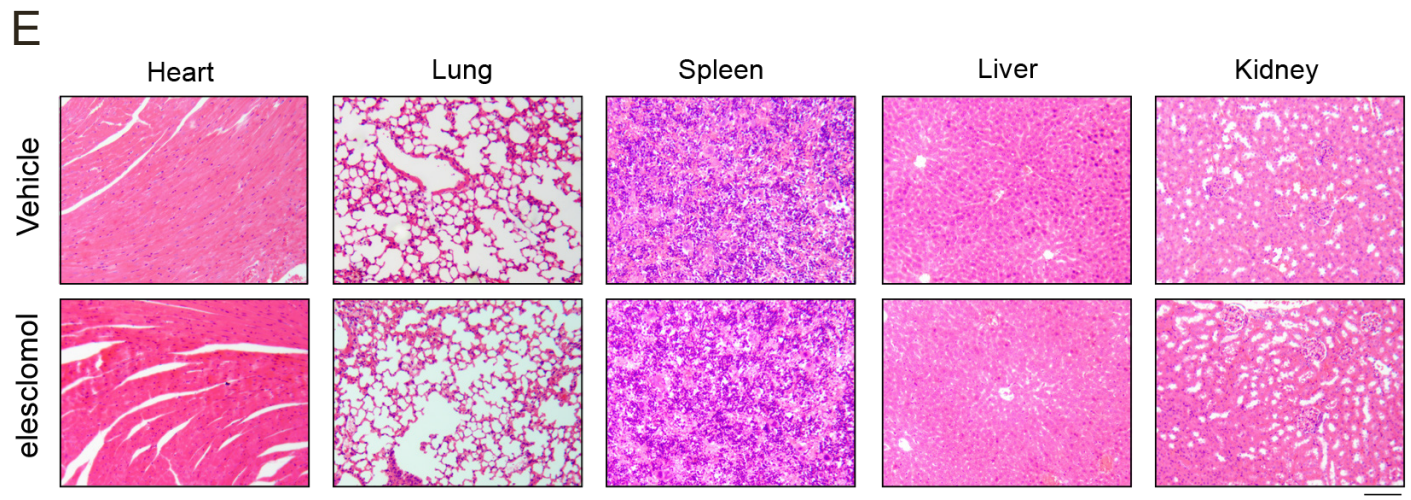

Supplementary Figure S6. Elesclomol suppressed the growth of ARID1A-deficient HCC tumours in vivo, related to Figure 6
(A) Staining and quantification of ARID1A, PKM, and the cell proliferation marker Ki67 in xenograft tumours harvested from CDX model mice (mean ±SD; n=3 independent experiments) ,Scale bar = 100 μm. ARID1A Enlarged, 25 μm.
(B) Alterations in mouse body weights following treatment with elesclomol in CDX model (mean ±SD; n=6 independent experiments).
(C) The expression of ARID1A in dissociated tumor derived from the PDX model was assessed.
(D) Alterations in mouse body weights following treatment with elesclomol in PDX model (mean ±SD; n=6 independent experiments).
(E) Representative images of H&E staining of heart, lung, liver, spleen, and kidney samples from vehicle or elesclomol treated PDX model mice, Scale bar = 100 μm.

Supplementary Tables S1. List of primer sequences used in this study, related to STAR methods

Primers used for RT-PCR	Forward	Reverse
β-actin	GAGAAAATCTGGCACCACACC	GGATAGCACAGCCTGGATAGCAA
PKM	CTGAAGGCAGTGATGTGGCC	ACCCGGAGGTCCACGTCCTC

Primers used for Cut&Run-qPCR	Forward	Reverse
PKM	TGCTGGCATGAGGAAAGAGG	TGTGCTTGTCTGCACGTAGG

siRNA sequences	Forward	Reverse
SDHA#1	GGCAGGGUUUAAUACAGCATT	UGCUGUAUUAAACCCUGCCTT
SDHA#2	CACACCUUAUAUGGAAGGUTT	ACCUUCCAUAUAAGGUGUGTT
ACO2#1	CAGGUGCAAUCGUGGAAUATT	UAUUCCACGAUUGCACCUGTT
ACO2#2	GGGAGAAGAACACAAUCGUTT	ACGAUUGUGUUCUUCUCCCTT
ARID1A	GCAGGAGCUAUCUCAAGAUTT	AUCUUGAGAUAGCUCCUGCTT